

# Cooling of neutron stars in soft X-ray transients with realistic crust composition

A.Y. Potekhin<sup>a</sup>, A.I. Chugunov<sup>a</sup>, N.N. Shchepochin<sup>b</sup>, M.E. Gusakov<sup>a</sup>

<sup>a</sup>*Ioffe Institute, Politeknicheskaya 26, Saint Petersburg, 194021, Russia*  
<sup>b</sup>*Institut d'Astronomie et d'Astrophysique, ULB, CP226, Brussels, 1050, Belgium*

---

## Abstract

Thermal radiation of neutron stars in soft X-ray transients (SXTs) in a quiescent state is believed to be powered by the heat deposited in the stellar crust due to nuclear reactions during accretion. Confronting observations of this radiation with simulations helps to verify theoretical models of the dense matter in neutron stars. We simulate the thermal evolution of the SXTs with theoretical models of the equation of state and composition of the accreted crust. The new family of such models were recently developed within a thermodynamically consistent approach by modeling the nuclear evolution of an accreted matter as it sinks toward the stellar center, starting from representative thermonuclear ash compositions. The crust cooling curves computed with the traditional and modern theory are compared with observations of SXTs MXB 1659–29 and IGR J17480–2446. We show that the new and traditional models of the accreted neutron star crusts are similar in their capability to explain the thermal evolution of neutron stars in SXTs. Both kinds of models require inclusion of additional ingredients not supplied by the current theory, such as the shallow heating and variation of thermal conductivity, to fit observations.

*Keywords:* stars: neutron, dense matter, X-rays: binaries, X-rays: individual: MXB 1659–29, IGR J17480–2446

---

## 1. Introduction

Many neutron stars (NSs) reside in binary systems and accrete matter from the companion. Some of them, called soft X-ray transients (SXTs), accrete intermittently, so that accretion episodes (outbursts) alternate with periods of quiescence, when accretion terminates or is strongly suppressed. The outbursts are revealed by intense X-ray radiation due to the release of the gravitational energy of matter falling from the accretion disk on a NS. In the quiescence, the X-ray luminosity decreases by orders of magnitude and may be determined by thermal emission from the NS surface (see, e.g., Wijnands et al. 2017 for a review).

The accretion during an outburst leads to nuclear reactions in the crust accompanied by heat release. Thermonuclear reactions in the outermost NS envelopes transform accreted protons or alpha particles into a complex mixture of heavy elements, called thermonuclear ashes. Most of the energy produced in these reactions is immediately irradiated in X-rays and neutrinos. According to the deep crustal heating scenario (Sato, 1979; Haensel and Zdunik, 1990), heat is also produced as the crust matter is pushed inside the star under the weight of newly accreted material. A part of the accumulated heat propagates from the NS crust to the core and the other part leaks through the surface. The so-called quasi-persistent SXTs have long outbursts (lasting months to years), which appreciably warm up the crust. Thermal relaxation of the overheated crust manifests itself by the decline of the observed thermal X-ray luminosity (e.g., Wijnands et al. 2017 and references therein).

An analysis of observations of the post-outburst cooling allows one to constrain the thermal conductivity and heat capacity of the crust (e.g., Rutledge et al. 2002; Shternin et al. 2007;

Page and Reddy 2013). Such an analysis is complicated. As a rule, interpretation of the observed crust cooling within the deep crustal heating scenario requires involving the so-called “shallow heating” by some additional energy sources at relatively low densities (Brown and Cumming, 2009). Besides, some SXTs may experience weak and variable residual accretion during quiescence (e.g., Turlione et al., 2015).

A traditional approach to calculation of the equation of state (EoS) and the heat release in the crust (Haensel and Zdunik, 1990, 2003, 2008; Fantina et al., 2018) is based on the assumption that free neutrons move together with the nuclei during accretion. Recently, the theoretical models of the accreted crust have been revised by Gusakov and Chugunov (2020, 2021, hereafter GC), who found that diffusion of free neutrons results in their redistribution over the inner crust, conforming to the hydrostatic and diffusion equilibrium condition (the nHD condition). Gusakov and Chugunov (2021) derived an universal formula for the total heating efficiency in the fully accreted inner crust in the nHD equilibrium. Shchepochin et al. (2021, 2022, 2023, hereafter SGC) performed a more detailed study of the composition, EoS, and heat release in the accreted crust with allowance for nuclear transformations during the accretion under the nHD equilibrium condition.

In a previous paper (Potekhin et al., 2023, hereafter Paper I) we performed numerical simulations of the thermal evolution of the SXTs in the nHD equilibrium and compared the results with the traditional approach and with observations. For the latter, we considered a collection of quasi-equilibrium thermal luminosities of the SXTs in quiescence (Potekhin et al., 2019) and also the NS crust cooling in SXT MXB 1659–29 (Parikh et al., 2019). We found that the observed quasi-stationary thermal lu-

minosities of the SXTs can be equally well fitted (within the observational uncertainties) using the traditional and thermodynamically consistent models, provided that the shallow heat diffusion into the core is taken into account. The observed crust cooling in MXB 1659–29 could also be fitted in the frames of both models, but the choice of the model affects the derived parameters responsible for the thermal conductivity in the crust and for the shallow heating.

The simulations in Paper I were based on the model of the composition and heating in the outer crust developed by Gusakov and Chugunov (2021, 2024). In this model, the nuclear transformations occur, starting from  $^{56}\text{Fe}$ , at some discrete values of pressure in the outer crust, at the interface between the outer and inner crusts, and near the interface between the inner crust and the core. In the present work, we explore the thermal evolution of SXTs during the outbursts and quiescence, using the most recent SGC calculations, which start with realistic compositions of thermonuclear ashes, instead of  $^{56}\text{Fe}$ , and are continued into upper layers of the inner crust. This update cannot affect the basic conclusions of Paper I concerning the quasi-stationary quiescent states of the SXTs, which depend mainly on the total time-averaged heat injected into the core during many consecutive outbursts, because a total deep crustal heating of the star is similar in the GC and SGC models. However, the individual crust cooling curves are sensitive to the positions and intensities of the discrete heating sources and to the details of the crust composition, therefore they could be substantially different for the different models.

In the present paper we perform numerical simulations of the thermal evolution of SXTs with the SGC crust models and compare the crust cooling curves with each other and with observations of SXTs MXB 1659–29 and IGR J17480–2446, whose luminosities in quiescent, active, and post-outburst cooling states have been well monitored. For these simulations we construct analytical fits to the EoS in the inner crust and compose tables of the deep crustal heating intensities and composition of the inner and outer crusts in the mean ion approximation.

The paper is organized as follows. In Section 2 we describe the accreted crust models used in this research. In Section 3 we describe the simulations of the thermal evolution of the SXTs MXB 1659–29 and IGR J17480–2446, compare these simulations with observations, and discuss the results. We summarize the conclusions in Section 4. Appendix A presents analytical fits to the pressure and the fraction of free neutrons in the inner crust, which are employed in the simulations.

## 2. Accreted crust models

Composition of the deep accreted NS crust depends on the initial composition in the shallow layers, which are pushed toward the stellar center during accretion. The initial composition is formed by thermonuclear burning of accreted elements in the NS envelope. The burning proceeds in different regimes (stable or unstable) depending on the composition of the accreted matter and the accretion rate. The SGC models of an accreted NS crust are based on three representative thermonuclear ash compositions. A composition presented by Cyburt et al. (2016),

based on the hydrodynamic code KEPLER (Woosley et al., 2004), has a wide distribution of elements with the most abundant nuclides being in the iron group. If there is a sufficiently large amount of hydrogen at the moment of burst ignition, the extended rapid proton capture process could lead to the formation of the palladium group elements (Schatz et al., 2001). Besides, some accreting NSs exhibit so-called superbursts, which originate from thermonuclear explosion of carbon accumulated in the crust and result in a narrow distribution of nuclides with a peak in the elements of the iron group (Keek and Heger, 2011). In the SGC approach, the composition and EoS of the accreted crust is found by tracing pathways of nuclear transformations with increasing pressure, using a nuclear reaction network and starting with one of these three thermonuclear ash compositions in shallow depths. The three respective models of the accreted crust are briefly called Kepler (K), Extreme rp (RP), and Superburst (SB) models.

The GC and SGC accreted crust models depend on the pressure  $P_{\text{oi}}$  at the interface between the outer and inner crust. Because of the diffusion of neutrons,  $P_{\text{oi}}$  may differ from the neutron-drip pressure for the pristine crust. The value of  $P_{\text{oi}}$  is currently unknown, and it is used as a free parameter in constructing the accreted crust models. Gusakov and Chugunov (2020, 2024) argued that  $P_{\text{oi}}$  should lie between the minimum value  $P_{\text{oi}}^{(0)}$ , which corresponds to the case where no heat is released in the deep layers of the inner crust beyond the scope of the detailed modeling, and maximum  $P_{\text{oi}}^{(\text{cat})}$ , which roughly equals the neutron-drip pressure in cold catalyzed matter. The pressure values, at which the nuclear transformations occur, as well as the values of  $P_{\text{oi}}^{(0)}$ ,  $P_{\text{oi}}^{(\text{cat})}$  and the amounts of heat released at each transformation, depend on the initial nuclear composition and on the employed nuclear models.

The SGC calculations were performed in frames of a simplified reaction network (Shchepochin et al., 2021) and employed theoretical mass tables for the finite-range droplet macroscopic model of nuclei FRDM12 (Möller et al., 2016). The values of  $P_{\text{oi}}^{(0)}$  for the K, RP, and SB models are  $7.26 \times 10^{29} \text{ dyn cm}^{-2}$ ,  $7.75 \times 10^{29} \text{ dyn cm}^{-2}$ , and  $7.29 \times 10^{29} \text{ dyn cm}^{-2}$ , respectively, and  $P_{\text{oi}}^{(\text{cat})}$  for the FRDM12 model equals  $7.86 \times 10^{29} \text{ dyn cm}^{-2}$ . The SGC calculations provide sets of K, RP, and SB crust models for  $P_{\text{oi}}$  values in the range  $6.4 \times 10^{29} \text{ dyn cm}^{-2} \leq P_{\text{oi}} \leq 10^{30} \text{ dyn cm}^{-2}$ , which embraces the interval  $[P_{\text{oi}}^{(0)}, P_{\text{oi}}^{(\text{cat})}]$ . For each  $P_{\text{oi}}$  value, there is a distribution of nuclei, depending on the outer crust composition. The latter has been computed and tabulated for the layers with  $P$  from  $6 \times 10^{26} \text{ dyn cm}^{-2}$  at  $\rho \approx (1.3 - 1.4) \times 10^9 \text{ g cm}^{-3}$  in the outer crust to  $P \approx 2 \times 10^{30} \text{ dyn cm}^{-2}$  at  $\rho = \rho_{\text{max}} \equiv 2 \times 10^{12} \text{ g cm}^{-3}$  in the inner crust. At certain pressure values, the nuclear transformations are accompanied by heat release.

In the present work we employ the mean ion approximation: we calculate the mean charge and mass numbers,  $\langle Z \rangle$  and  $\langle A \rangle$ , from the detailed tables obtained by SGC and plug them into the analytical formulae for thermodynamic functions, thermal conductivities, and neutrino emissivities (Potekhin et al., 2015, and references therein). Here and hereafter, the angle brackets denote an average with weights proportional to number fractions of the nuclei. In addition to  $\langle Z \rangle$  and  $\langle A \rangle$ , the thermal conductiv-

ities depend on the “impurity parameter”  $Q_{\text{imp}} \equiv \langle (Z - \langle Z \rangle)^2 \rangle$ , which is also obtained from the detailed SGC tables. At shallow depths above the first nuclear transformation ( $P \lesssim 6 \times 10^{26}$  dyn cm $^{-2}$ ,  $\rho \lesssim 1.4 \times 10^9$  g cm $^{-3}$ ), we assume the same composition as in the initial mixture of the specific model. In particular, the initial composition affects the temperature profile in the heat blanketing envelope, making the relation between the internal temperature in the core and the effective surface temperature  $T_{\text{eff}}$  in quiescence slightly different for the different ash models. The fraction of free neutrons and the EoS in the inner crust are given by the analytical fitting formulas in Appendix A. These fits provide a good accuracy in the entire range of the densities covered by the SGC data for the inner crust,  $\rho_{\text{oi}+} < \rho < \rho_{\text{max}}$ , where  $\rho_{\text{oi}+}$  is the density at the outer edge of the inner crust.

In the deeper crust layers, at  $\rho > \rho_{\text{max}}$ , the numerical SGC data are absent. It turns out, however, that the different EoSs, corresponding to different values of  $P_{\text{oi}}$ , become close to the EoS model BSk24 (Pearson et al., 2018) with increasing  $\rho$  towards  $\rho_{\text{max}}$ . Therefore, for the sake of the NS modeling, we extend the fitted EoS at  $\rho > \rho_{\text{max}}$  using the BSk24 EoS, modified by a constant shift of pressure. This shift is applied so as to get a continuous  $P(\rho)$  at the matching point:  $P(\rho)|_{\rho > \rho_{\text{max}}} = P_{\text{BSk24}}(\rho) + P_{\text{fit}}(\rho_{\text{max}}) - P_{\text{BSk24}}(\rho_{\text{max}})$ , where  $P_{\text{fit}}$  is the fit (A.1) for the SGC EoS and  $P_{\text{BSk24}}$  is the fit of Pearson et al. (2018) for the BSk24 EoS. Examples of the resulting EoS are shown in the upper panel of Fig. 1. For comparison, three unified EoSs of the cold catalyzed crust are also shown: BSk22, BSk24, and BSk25 (Pearson et al., 2018), which differ by the assumed nuclear symmetry energy at the nuclear saturation density (32 MeV, 30 MeV, and 29 MeV, respectively). The lower panel demonstrates the logarithmic derivative  $\chi_\rho \equiv d \log P / d \log \rho$ . The matching point manifests itself by a break of  $\chi_\rho$  (encircled). The break is rather small, and the extended EoS fits to the accreted crust models become indistinguishable from the BSk24 EoS at large densities  $\rho \gg \rho_{\text{max}}$ . The same EoS was employed to describe the pure neutron matter outside clusters in SGC models.

In the upper panel of Fig. 2 we compare predictions of one traditional model and two nHD-consistent models GC and SGC for the heat generated per accreted baryon,  $E_h$ , integrated from the surface to a given density in the crust, as a function of mass density. As an example of a traditional model (without the nHD equilibrium), we have chosen the relatively recent and advanced model by Fantina et al. (2018), specifically its version consistent with the BSk24 energy density functional (for short, the F+18 model). As an example of the GC model, we have chosen the version that is consistent with the BSk24 energy density functional and assumes  $P_{\text{oi}} = P_{\text{oi}}^{(\text{cat})} = 7.731 \times 10^{29}$  dyn cm $^{-2}$ . The SGC models are presented by the SB ashes version with  $P_{\text{oi}} = P_{\text{oi}}^{(\text{cat})}$ .

The heating function  $E_h(\rho)$  is qualitatively similar for the GC and SGC models, although the SGC model reveals more details: there are more heating layers in the outer crust (at  $\rho < \rho_{\text{oi}} \sim 4 \times 10^{11}$  g cm $^{-3}$ ) and, in addition, some heating sources in the upper part of the inner crust (at  $\rho_{\text{oi}} < \rho < \rho_{\text{max}}$ ). The lower panel of Fig.2 presents a comparison of the functions  $E_h(\rho)$  for the K, RP and SB versions of the SGC model with  $P_{\text{oi}} = P_{\text{oi}}^{(\text{cat})}$

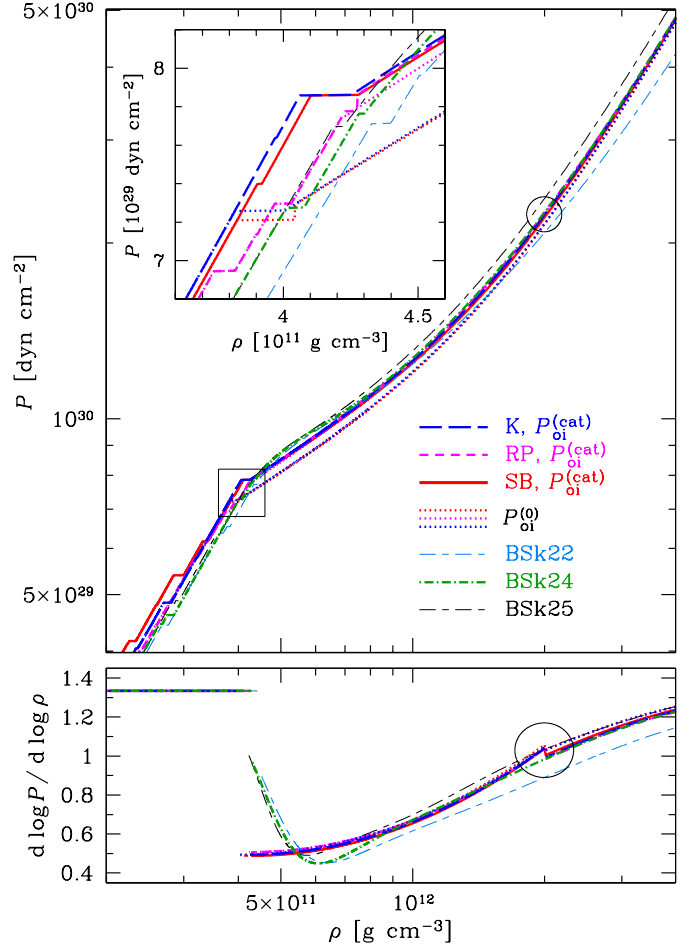


Figure 1: EoS models. *Upper panel*: Pressure  $P$  as function of mass density  $\rho$  is plotted according to the tabular composition in the outer crust and analytic fits in the inner crust, extended beyond the computed data range as explained in the text. Red solid, magenta short-dashed, and blue long-dashed lines show the EoS with the Kepler (K), Extreme rp (RP), and Superburst (SB) models for the accreted crust, respectively, with  $P_{\text{oi}} = P_{\text{oi}}^{(\text{cat})}$ . The dotted curves of the respective colors correspond to the same models with  $P_{\text{oi}} = P_{\text{oi}}^{(0)}$ . For comparison, the EoSs of cold catalyzed NS matter are shown: BSk24 (dot-dashed line), BSk22 and BSk25 (lower and upper thin long-and-short-dashed lines). The inset shows a zoom to the vicinity of the outer-inner crust interface, selected by the rectangle. *Lower panel*: Logarithmic derivative of pressure with respect to the density for the same EoS models. The gaps correspond to the outer-inner crust interface. In both panels, the circle highlights the region of maximum  $P$  and  $\rho$  values for the computed SGC data, where the fit to the data is matched by a shifted BSk24 EoS (see text).

and  $P_{\text{oi}} = P_{\text{oi}}^{(0)}$ .

A total deep crustal heating of the star,  $E_h^{(\text{tot})}$  is given by  $E_h$  at  $\rho \geq \rho_{\text{cc}}$ , where  $\rho_{\text{cc}} \sim (1 - 2) \times 10^{14}$  g cm $^{-3}$  is the density of the crust-core interface. It is given by the line segments near the right axes in Fig. 2. We see that the GC and SGC models predict  $E_h^{(\text{tot})}$  in the range of  $\sim 0.2 - 0.6$  MeV per an accreted baryon. It is much weaker than in the traditional models (such as F+18), which predict  $E_h^{(\text{tot})} \sim (1.5 - 2)$  MeV. In Paper I, we have already examined the influence of such a difference in  $E_h^{(\text{tot})}$  on the quasi-stationary thermal states of the SXTs in quiescence. The effect of this difference turned out to be not very large in view of the observational and theoretical uncertainties. In particular,

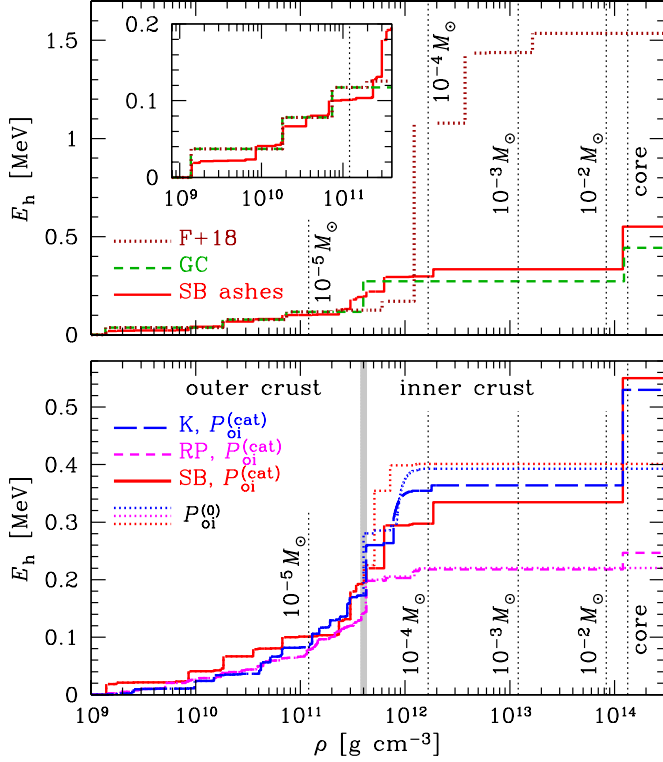


Figure 2: *Upper panel*: Total heat  $E_h$ , generated per accreted baryon in a layer from the star surface to a given mass density  $\rho$ , according to the model of Fantina et al. (2018) (F+18, dotted line), the model of Gusakov and Chugunov (2021) with  $P_{oi} = P_{oi}^{(cat)}$  (GC, dashed line), and the model of Shchechilin et al. (2023) with  $P_{oi} = P_{oi}^{(cat)}$  for the SB ashes (solid line). The gaps on the lines (best visible in the F+18 case) are due to the density jumps at the interfaces between neighboring layers containing different nuclei. The vertical dotted lines mark the  $\rho$  values corresponding to the mass of overlying material, from  $10^{-5} M_\odot$  to  $10^{-2} M_\odot$ , labeled near these lines, for a NS with mass  $M = 1.6 M_\odot$  and radius  $R = 12.6$  km, which corresponds to BSK24 EoS in the core. *Lower panel*: The same for six SGC models: K, RP, and SB with  $P_{oi} = P_{oi}^{(cat)}$  (long-dashed blue, short-dashed magenta, and solid red lines, respectively) and with  $P_{oi} = P_{oi}^{(0)}$  (dotted lines of the respective colors). The vertical gray strip shows the range of the density at outer-inner crust boundary for the selected models,  $\rho_{oi} \approx (3.8 - 4.3) \times 10^{11} \text{ g cm}^{-3}$ .

the effect is smeared by the shallow heating, which contributes in warming up the NS core due to the heat transport through the crust. Clearly, the effect of the difference between the GC and SGC models on the quasi-stationary SXT states should be still smaller than the effect of their difference from the traditional models. For this reason, in the present work we do not study the quasi-stationary thermal states of the SXTs, but focus on the dynamics of post-outburst crustal cooling.

### 3. Cooling of SXT crusts

To explore the thermal evolution of the SXT crusts with the SGC models, we have chosen two SXTs, MXB 1659–29 and IGR J17480–2446, whose crust cooling observations are sufficiently complete to reduce a number of uncertainties: their crustal cooling has been well monitored, the start and end dates of the outbursts are known, quasi-equilibrium effective temper-

atures are measured with a sufficient accuracy, and average accretion rates during outbursts have been estimated. We perform numerical simulations of the crust heating during an outburst and the subsequent cooling during quiescence, using the code described in Potekhin and Chabrier (2018) with essentially the same physics input as in Paper I, except for the new crust models.

#### 3.1. MXB 1659–29

The SXT MXB 1659–29 (MXB 1658–298, MAXI J1702–301) is a good touchstone for testing crust cooling models, because it has been observed for a long time, revealed three outbursts, and has a well documented record of the crust cooling after the last two of them (see Parikh et al. 2019 and references therein). As in Paper I, the accretion episodes observed in 1976–1979, 1999–2001, and 2015–2017 will be named *outburst 0*, *outburst I*, and *outburst II*, respectively. The crust cooling after the end of outburst I was simulated in a number of works (Brown and Cumming, 2009; Cackett et al., 2013; Deibel et al., 2017; Parikh et al., 2019; Potekhin and Chabrier, 2021; Mendes et al., 2022; Potekhin et al., 2023; Allard and Chamel, 2024a,b). A consistent modeling of the short-term evolution of MXB 1659–29 during and after both outbursts I and II was performed in Parikh et al. (2019); Potekhin and Chabrier (2021), and in Paper I. Here the term *consistent modeling* (following Parikh et al., 2019) means that all model parameters are kept fixed and the same during and after different outbursts (Allard and Chamel 2024b modeled the two bursts separately, without requiring the constancy of the parameters).

The simulation procedure is similar to that in Potekhin and Chabrier (2021) and in Paper I. Starting from a quasi-steady thermal structure of the NS with a sufficiently hot interior, we simulate passive cooling until the observed quasi-equilibrium luminosity in quiescence is reached. For the latter, we fix the effective temperature  $\tilde{T}_{\text{eff}}$  at a level consistent (within uncertainties) with observations of the SXT in quiescence. Here, tilde indicates that the quantity is corrected for gravitational redshift. The stellar mass was fixed,  $M = 1.6 M_\odot$ , to agree with quiescent luminosity of MXB 1659–29 for average accretion rate, see figure 2 in Paper I. For the BSK24 EoS in the core, it results in the stellar radius  $R \approx 12.6$  km.

Let us note that the last observation before outburst II (in 2012, after  $t = 10.8$  yr of cooling) gave contradictory results, reported by Cackett et al. (2013): the same spectral analysis as for the observations at  $t = 6.6$  yr (Cackett et al., 2008) suggested  $\tilde{T}_{\text{eff}}$  consistent with the preceding result, but the count rate dropped. The authors tried different spectral models by allowing the hydrogen column density  $N_H$  to differ from the preceding value or by including a power-law spectral component in addition to the thermal one, and obtained estimates of  $k_B \tilde{T}_{\text{eff}}$  (where  $k_B$  is the Boltzmann constant) ranging from  $43 \pm 5$  eV to  $56 \pm 2$  eV. Here we adopt the quasi-stationary level at  $k_B \tilde{T}_{\text{eff}} = 54$  eV, compatible with the observations at  $t = 6.6$  yr (Cackett et al., 2008).

Then we simulate outburst 0, assuming it to be the same as outburst I, during 2.5 years, followed consecutively by 20 years

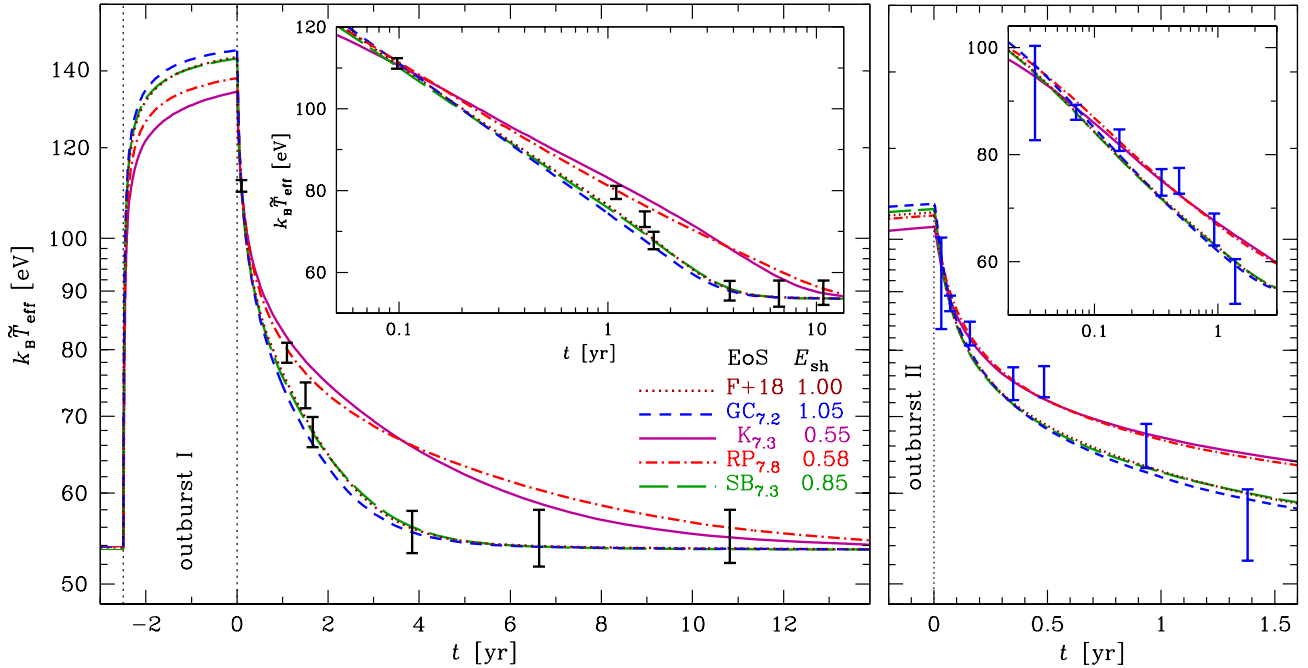


Figure 3: Simulated light curves for the outbursts I (*left panel*) and II (*right panel*) of MXB 1659–29 versus observations. The redshifted effective temperature in energy units  $k_B \tilde{T}_{\text{eff}}$  is shown as function of time  $t$ , counted from the end of an outburst. The dotted line is calculated assuming the F+18 model, and the other four lines represent different nHD-consistent models with  $P_{\text{oi}} = P_{\text{oi}}^{(0)}$ . The short-dashed line represents the results for the GC model, while the solid, dot-dashed, and long-dashed lines correspond to the SGC models K, RP, and SB. The subscripts at the symbols GC, K, RP, and SB in the legend indicate the approximate values of  $P_{\text{oi}29}$  for the shown models. The vertical errorbars (black and blue for the crust cooling after outbursts I and II respectively) show the spectral fitting results from Parikh et al. (2019) at the 90% confidence, except for the bar at  $t = 10.8$  yr in the left panel, which represents one of the different estimates by Cackett et al. (2013, see text). The vertical dotted lines separate the crust heating during an outburst from the passive cooling during the quiescence. The insets show the same dependences and data at another scale for the crust cooling stage only.

in quiescence, then by the outburst I, by 14 years of quiescence, by 1.52 years of outburst II, and by present day quiescence. The accretion rate during outburst I is adopted at the level  $\dot{M}_I = 4 \times 10^{-9} M_{\odot} \text{ yr}^{-1}$ , in accordance with the estimate  $\dot{M}_I = (4 \pm 2) \times 10^{-9} M_{\odot} \text{ yr}^{-1}$  in Potekhin and Chabrier (2021). The large uncertainty of this estimate is mainly related to the uncertainty in the distance to this SXT, which can be  $9 \pm 2$  kpc or  $12 \pm 3$  kpc depending on the assumed composition of thermonuclear fuel in its X-ray bursts (Galloway et al., 2008).

The observed accretion rate during outburst II is known to vary strongly, but we simplify the model by adopting the constant rate  $\dot{M}_{\text{II}} = 1.8 \times 10^{-9} M_{\odot} \text{ yr}^{-1}$ , as it provides the best fits of the simulated cooling curves to the observations of the crust cooling after outburst II and roughly agrees with Fig. 1 of Parikh et al. (2019), which suggests the average accretion rate ratio  $\langle \dot{M}_{\text{II}} \rangle / \langle \dot{M}_I \rangle \sim 1/3 - 1/2$ . The crust composition and shallow heating parameters are kept the same for all three outbursts and cooling periods for each simulation set.

In most of our previous simulations of the thermal evolution of MXB 1659–29, we assumed the position of the shallow heating coincident with the position of the shallowest of the deep heating sources at  $\rho \approx 1.4 \times 10^9 \text{ g cm}^{-3}$ . Here we adopt the same rule. In Paper I we demonstrated that one can produce almost identical light curves by decreasing the depth of the shallow heating layer to  $\rho \sim 10^8 \text{ g cm}^{-3}$  with simultaneous increase of the shallow heating power by 30–40%. We adjusted

the shallow heating energy per baryon,  $E_{\text{sh}}$ , so as the light curve matched the first observation after outburst I (at  $t \approx 0.1$  yr).

In Fig. 3 we compare the light curves calculated using the traditional model F+18, a GC model, and SGC models K, RP, and SB with observations. For the GC and SGC models, we used the parameters  $P_{\text{oi}} = P_{\text{oi}}^{(0)}$  (approximate values of  $P_{\text{oi}29} \equiv P_{\text{oi}}/10^{29} \text{ dyn cm}^{-2}$  are marked by the subscripts in the legend). We show the effective temperature corresponding to the thermal flux from the outer crust to the surface during and after the outbursts I and II, discarding the instantaneous energy release near the NS surface due to the accretion during an outburst. In each case, time is counted from the end of the outburst:  $t = 0$  corresponds to MJD 52162 and 57809.7 for outbursts I and II, respectively (Parikh et al., 2019). The vertical errorbars are the observational estimates at the 90% confidence level (Parikh et al., 2019). For the observation at  $t = 10.8$  yr after outburst I, we show the estimate  $k_B \tilde{T}_{\text{eff}} = 55 \pm 3 \text{ eV}$ , obtained by Cackett et al. (2013) using a spectral model with free  $N_{\text{H}}$  but without a power-law component.

The models F+18 and SB produce cooling curves, compatible with most observations, except for the ones at  $t = 1.1$  yr after outburst I and at  $t = 0.5$  yr after outburst II, for which the errorbars lie significantly higher than the curves. Although the F+18 and SB curves are almost identical, they are produced using different shallow heating,  $E_{\text{sh}} = 1 \text{ MeV}$  and  $0.85 \text{ MeV}$ , respectively. The smaller value in the SB case is needed to match

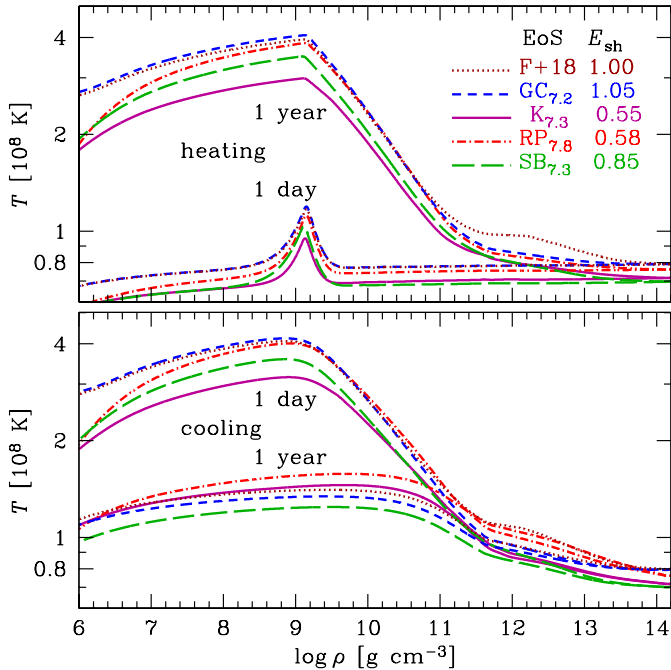


Figure 4: Temperature profiles during the outburst I (upper panel) and subsequent cooling (lower panel) at 1 day and 1 year after the start of the heating and the cooling, respectively. The same NS models as in Fig. 3 are shown with the same line styles.

the early cooling observation, because of the smaller conductivity due to the non-zero impurity parameter  $Q_{\text{imp}}$ , corresponding to a mixture of different nuclei. Indeed, it is known that an increase of  $Q_{\text{imp}}$  requires a decrease of  $E_{\text{sh}}$  to match the same early cooling data (cf. Paper I).

The GC model with  $Q_{\text{imp}} = 0$  requires a larger  $E_{\text{sh}}$  and produces a quicker crustal cooling because of the absence of heating sources in the upper layers of inner crust. Conversely, the K and RP models require a weaker shallow heating and produce a slower cooling because of their much larger  $Q_{\text{imp}}$  (see Fig. 4 in Shchechilin et al. 2023). The latter two models appear to be incompatible with observations of outburst I (left panel of Fig. 3).

Fig. 4 provides an insight into the thermal structure of the NS models shown in Fig. 3. We see that this structure is dominated by the shallow heating. The slightly different temperatures at high densities ensure the same quasi-equilibrium  $T_{\text{eff}}$  for different models in quiescence, because of the different composition of the heat blanketing envelopes, as mentioned in Section 2.

In Fig. 5 we compare the post-outburst cooling for several modifications of the K and SB models (the results for RP models are similar to those for the K models). The curves marked  $\text{SB}_{7.3}$  and  $\text{K}_{7.3}$  are the same as in Fig. 3. The models  $\text{SB}_{8.3}$  and  $\text{K}_{7.9}$  are characterized by larger  $P_{\text{oi}}$ . According to SGC, the increase of  $P_{\text{oi}}$  is accompanied by changes of the impurity parameter in the inner crust:  $Q_{\text{imp}}$  at  $\rho = \rho_{\text{max}}$  is increased from 1.2 to 3.0 in the SB case and decreased from 5.4 to 3.8 in the K case. By default we keep  $Q_{\text{imp}}$  at  $\rho > \rho_{\text{max}}$  equal to its value at  $\rho = \rho_{\text{max}}$ . This may be an overestimation, because  $Q_{\text{imp}}$  demonstrates a decrease towards high densities. To test a possible ef-

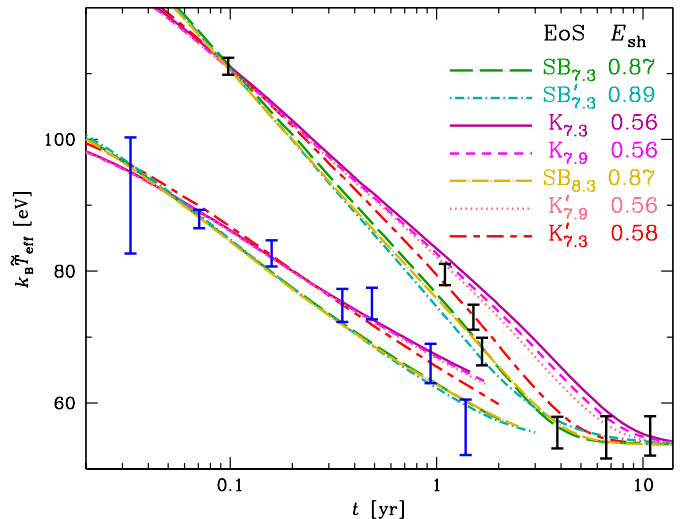


Figure 5: Simulated light curves for the crust cooling after the outbursts I (upper curves and black errorbars) and II (lower curves and blue errorbars) of MXB 1659–29 versus observations. The data and curves denoted  $\text{SB}_{7.3}$  and  $\text{K}_{7.3}$  are the same as in Fig. 3. The other curves are variations of the K and SB models, denoted according to the legend:  $\text{K}_{7.9}$  and  $\text{SB}_{8.3}$  are the models with higher  $P_{\text{oi}}$ ,  $\text{SB}'_{7.3}$  is characterized by a suppressed neutron superfluidity,  $\text{K}'_{7.9}$  is characterized by a suppressed parameter  $Q_{\text{imp}}$  in deep layers of the crust, and  $\text{K}'_{7.3}$  is a model with a thin accreted crust (see text for details).

fect of this overestimation, we consider the model  $\text{K}'_{7.9}$ , which differs from  $\text{K}_{7.9}$  by setting  $Q_{\text{imp}}$  to zero at  $\rho > \rho_{\text{max}}$ . The model  $\text{SB}'_{7.3}$  differs from  $\text{SB}_{7.3}$  by suppressing the singlet neutron superfluidity, which leads to an increase of the specific heat in the inner crust. We see that these modifications have minor effects on the crust cooling curves. In all the cases the SB models, which have relatively small  $Q_{\text{imp}}$ , tend to underestimate the effective temperature at intermediate crust cooling times, while the K models, which have relatively large  $Q_{\text{imp}}$ , tend to overestimate it.

Finally, we test the possibility that the reprocessed accreted matter replaces the cold catalyzed matter only in the upper layers of the crust to some density  $\rho_{\text{ac}} < \rho_{\text{cc}}$  (see Wijnands et al., 2013; Fantina et al., 2018; Potekhin et al., 2019). The model  $\text{K}'_{7.3}$  is constructed for the K composition with  $P_{\text{oi}} = P_{\text{oi}}^{(0)}$ , as in the model  $\text{K}_{7.3}$ , but only at  $\rho < \rho_{\text{ac}} = 10^{11} \text{ g cm}^{-3}$ . At larger densities, the BSk24 model is used. The restriction of the accreted layer by the relatively small densities accelerates the cooling, because thermal diffusion from shallow layers proceeds relatively quickly. For this reason, the above-mentioned overestimation of the effective temperature is reduced, so that the cooling curves for the model with a partially accreted crust  $\text{K}'_{7.3}$  are in better agreement with observations than the  $\text{K}_{7.3}$  curves for the fully accreted crust.

### 3.2. IGR J17480–2446

The SXT IGR J17480–2446 (Ter 5 X-2) is located in the globular cluster Terzan 5. The distance to this cluster is known ( $d = 5.5 \pm 0.9 \text{ kpc}$ , Ortolani et al., 2007), which reduces uncertainties in the analysis. This SXT revealed a relatively short (11 weeks, as estimated by Degenaar and Wijnands 2011) outburst

in 2010. It is the only outburst confidently identified from this source.<sup>1</sup>

The crust of the NS in IGR J17480–2446 had not yet been relaxed by the time of its last published observation, but its quasi-equilibrium effective temperature  $k_B \tilde{T}_{\text{eff}} = 77.7 \pm 2.0$  eV is known due to pre-outburst observations in 2003 and 2009 (Ootes et al., 2019). This makes it one of the hottest NSs in SXTs for their mean accretion rates. Another remarkable peculiarity of this NS is its spin period of 90 ms (Papitto et al., 2011), which corresponds to order of magnitude slower rotation, than in other SXTs with known NS spin periods.

The hot quasi-equilibrium state of this NS prompts that it does not experience the rapid cooling via the direct Urca processes. For the EoS model BSk24, which we use in the core of the NS, these processes work for stellar masses above  $1.595 M_\odot$  (Pearson et al., 2018). In the following we adopt a slightly smaller mass than in Section 3.1,  $M = 1.59 M_\odot$ , which is below this threshold. Otherwise the simulations of the thermal evolution are performed in the same way as in Section 3.1.

The results are shown in Fig. 6. The first three lines (without a prime in the legend) are for the SGC models K, RP, and SB with  $P_{\text{oi}} = P_{\text{oi}}^{(0)}$ . While the first observational result (at  $t = 0.15$  yr) is matched by adjusting  $E_{\text{sh}}$ , these crust cooling curves strongly underestimate  $\tilde{T}_{\text{eff}}$  for the later observations.

The slow post-outburst cooling is a known problem for this source. It was first noted by Ootes et al. (2019), who analyzed the crust cooling of IGR J17480–2446 using a traditional (Haensel and Zdunik, 2008) model of the accreted crust. These authors managed to achieve an agreement between the theory and observations by introducing a layer with an unusually low thermal conductivity at densities  $10^{11} \text{ g cm}^{-3} < \rho < 10^{12} \text{ g cm}^{-3}$ . The suppression of the conductivity was implemented by using a large impurity parameter  $Q_{\text{imp}}$  in this layer. They obtained an acceptable agreement between the theory and observations when using  $Q_{\text{imp}} \gtrsim 500$ , the best-fit values being around  $Q_{\text{imp}} \sim 1500$ .

The suppression of conductivity in the crust may arise due to the lack of long order in positions of the ions, as in an amorphous solid (a glass). The phonon spectrum is strongly disordered in this case. We therefore set a lower limit to the conductivity by treating the ions as if they were liquefied (cf. Brown, 2000). This can be roughly modeled by setting  $Q_{\text{imp}} = \langle Z \rangle^2$ . From physical point of view, it corresponds to the treatment of all ions as independent scatterers, and within the kinetic theory it is equivalent to the assumption that the structure factor  $S \equiv 1$ . The smallest discrepancy between the observations of IGR J17480–2446 and the crust cooling curves based on the SGC models is obtained, if such an amorphous layer is located

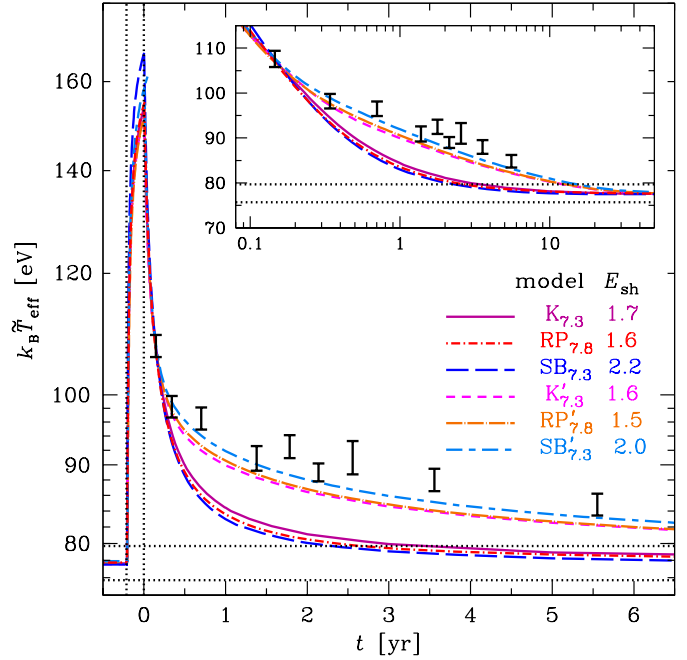


Figure 6: Simulated light curves for the NS in IGR J17480–2446 compared with observations of its crust cooling. The models  $K_{7.3}$ ,  $RP_{7.8}$ , and  $SB_{7.3}$  show the SGC models with  $P_{\text{oi}} = P_{\text{oi}}^{(0)}$ , analogous to such models in Fig. 3. The models  $K'_{7.3}$ ,  $RP'_{7.8}$ , and  $SB'_{7.3}$  are basically the same, but a layer with a suppressed thermal conductivity is introduced at  $3 \times 10^{10} \text{ g cm}^{-3} < \rho < 3 \times 10^{11} \text{ g cm}^{-3}$  (see text). The inset shows the same dependences and data at another scale for the crust cooling stage only. The vertical dotted lines mark the start and end of the outburst and the horizontal dotted lines mark the bounds on the quasi-equilibrium effective temperature observed before the outburst, according to Ootes et al. (2019) (at the  $1\sigma$  confidence level).

between the mass densities  $\sim 3 \times 10^{10} \text{ g cm}^{-3}$  and  $\sim 3 \times 10^{11} \text{ g cm}^{-3}$ , that is near the bottom of the outer crust. The light curves, simulated with such an amorphous layer, are marked in the legend of Fig. 6 by prime ( $K'$ ,  $RP'$ ,  $SB'$ ). We note in passing that models assuming the entire outer crust in the amorphous state, as well as those with an amorphous inner crust (as proposed by Jones 1999, 2001) did not provide us with an acceptable agreement between our crust cooling simulations and the observations.

#### 4. Conclusions

We employed the new set of NS accreted crust models SGC (Shchechilin et al., 2021, 2022, 2023), obtained for realistic nuclear mixtures under the nHD condition, to simulate heating and cooling of NSs during and after outbursts of SXTs MXB 1659–29 and IGR J17480–2446. Unlike the past analyses, which treated the impurity parameter of the crust  $Q_{\text{imp}}$  as free (sometimes density-dependent) fitting parameter and where the composition of the outer heat-blanketing NS envelopes arbitrarily varied, we consistently adopted these ingredients of the cooling theory directly from the underlying SGC models, thus reducing the number of degrees of freedom in the fitting.

<sup>1</sup>As noted by Ootes et al. (2019) (see also Heinke et al. 2024), some of the old outburst activity observed from the direction of Terzan 5 may have been due to IGR J17480–2446 as well, but the spatial resolutions of the earlier X-ray missions were not sufficient to resolve sources in dense globular cluster cores. Here we do not include this possibility into the analysis. The average accretion rate during the outburst was estimated to be  $0.11 \dot{M}_{\text{Edd}} \approx 3 \times 10^{-9} M_\odot \text{ yr}^{-1}$ , where  $\dot{M}_{\text{Edd}}$  is the Eddington accretion rate (Degenaar and Wijnands, 2011; Ootes et al., 2019). Thus the mean accretion rate over  $\sim 30$  years of observations is  $\sim 2 \times 10^{-11} M_\odot \text{ yr}^{-1}$  (Potekhin et al., 2019).

The observed cooling episodes for MXB 1659–29 (Parikh et al., 2019) were analyzed consistently, with NS crust parameters for the last cooling episode tied to those for the previous one. We found that the SB models can generate the crust cooling curves that are compatible with the results of observations of this SXT. As well as in the previous studies, this agreement between the theory and observations requires an adjustable heating source at a shallow depth (the shallow heating), in addition to the deep crustal heating predicted by the theory.

A previous analysis of the observed crust cooling of the NS in IGR J17480–2446 (Ootes et al., 2019) revealed that the theoretical cooling curves could not match observations without introducing a restricted layer with strongly suppressed thermal conductivity near the outer-inner crust transition. We eliminate the freedom in the conductivity suppression by assuming that it arises from a structural disorder, rather than from the difference in the nuclear composition. Thus we continue to use the SGC models of the crust composition, but assume that some layer of the crust is amorphous and has a low conductivity, which is estimated assuming that ions are independent scatterers ( $Q_{\text{imp}} = \langle Z \rangle^2$ ). In our modeling, the best-fit position of this layer is estimated to be near the bottom of the outer crust.

Thus the SGC models are similar to the traditional models of the accreted NS crusts in their capability to explain the thermal evolution of NSs in SXTs. Both the traditional and SGC models can serve as the base for constructing the heating and cooling curves of such NSs compatible with observations, but only with inclusion of additional ingredients not supplied by the current theory, such as the shallow heating and reduction of thermal conductivity.

## Funding

This research is partly supported (A.Y.P., A.I.C., M.E.G.) by the Russian Science Foundation Grant No. 22-12-00048. The work of N.N.S. was financially supported by the FWO (Belgium) and the Fonds de la Recherche Scientifique (Belgium) under the Excellence of Science (EOS) programme (project No. 40007501).

## CRediT authorship contribution statement

**A.Y. Potekhin:** Conceptualization, Methodology, Software – simulation of NS structure and thermal evolution, Formal analysis, Investigation, Visualization, Writing – original draft, Writing – review & editing. **A.I. Chugunov:** Conceptualization, Investigation, Writing – review & editing, Project administration. **N.N. Shchechilin:** Software – calculation of accreted crust composition and heating rates, Formal analysis, Investigation, Writing – review & editing. **M.E. Gusakov:** Conceptualization, Software – calculation of accreted crust composition and heating rates, Writing – review & editing.

Table A.1: Fit parameters in Eq. (A.1)

Ashes model	$a_1$	$a_2$	$a_3$
Kepler	0.494	−0.278	0.760
Extreme rp	0.507	−0.376	0.861
Superburst	0.488	0.021	0.433

## Declaration of competing interest

The authors declare that they have no known competing financial interests or personal relationships that could have appeared to influence the work reported in this paper.

## Data availability

The tables of the NS crust parameters  $\langle Z \rangle$ ,  $\langle A \rangle$ ,  $Q_{\text{imp}}$ , and heat release per accreted baryon  $E_{\text{h}}$  for the SGC models, which are employed in our calculations, are available at the URL <http://www.ioffe.ru/astro/NSG/ac crust/>. The other data pertinent to this research will be made available on request.

## Appendix A. Analytical fits for the accreted inner crust

We have constructed analytical fitting formulas for evaluation of the pressure  $P$ , density  $\rho$ , and fraction of free neutrons  $Y_{\text{nf}}$  in the inner crust, according to the SGC models. The original numerical data for each of the three models (K, RP, and SB) and each value of  $P_{\text{oi}}$  ( $6.4 \times 10^{29} \text{ dyn cm}^{-2} \leq P_{\text{oi}} \leq 10^{30} \text{ dyn cm}^{-2}$  with the step  $\Delta P_{\text{oi}} = 10^{28} \text{ dyn cm}^{-2}$ ) cover the density range  $\rho_{\text{oi}+} \leq \rho \leq \rho_{\text{max}} = 2 \times 10^{12} \text{ g cm}^{-3}$ , where  $\rho_{\text{oi}+}$  is the density at the upper edge of the inner crust (at  $P = P_{\text{oi}}$ ). In this density range, pressure logarithm is fitted by the formula

$$\log(P/P_{\text{oi}}) = a_1 x + b x^3, \quad (\text{A.1})$$

where

$$x = \log(\rho/\rho_{\text{oi}+}), \quad b = a_2 + a_3 \log P_{\text{oi}29}, \quad (\text{A.2})$$

$P_{\text{oi}29} \equiv P_{\text{oi}}/(10^{29} \text{ dyn cm}^{-2})$ , and the fit parameters  $a_i$  are given in Table A.1. The fit reproduces the calculated  $P$  values with a typical accuracy  $\sim 1\%$  and a maximum discrepancy of  $2\%$  for all three model families and all 37 values of  $P_{\text{oi}}$ .

Equation (A.1) has the form of a depressed cubic equation, which allows an analytical inversion, providing a fit of  $\rho$  as a function of  $P$ . The maximum error of this inverse fit lies within  $3.5\%$ .

The boundary density  $\rho_{\text{oi}+}$  in Eq. (A.1) is the upper end of the density jump at the transition from the outer crust to the inner crust. The lower end of this jump,  $\rho_{\text{oi}-}$ , can be considered as the bottom density of the outer crust. Both these densities are reproduced as functions of  $P_{\text{oi}}$  by the piecewise power law

$$\rho_{\text{oi}\pm} = c_{\pm} P_{\text{oi}29}^{3/4}, \quad (\text{A.3})$$

where the factors  $c_{\pm}$  are constant in certain intervals of  $P_{\text{oi}}$ . The values of  $c_{\pm}$  in Table A.2 provide the accuracy of  $\rho_{\text{oi}\pm}$  within  $0.15\%$  at most (typically  $\sim$  a few  $\times 0.01\%$ ).



Table A.2: Values of factors  $c_{\pm}$  in Eq. (A.3), in units of  $10^{11} \text{ g cm}^{-3}$ .

$P_{\text{oi}29}$	$c_{-}$	$P_{\text{oi}29}$	$c_{+}$
Kepler			
6.4 – 7.8	0.8577	6.4 – 8.3	0.9057
7.9 – 8.8	0.8627	8.4 – 8.9	0.9251
8.9	0.8671	9.0 – 10	0.9224
9.0 – 9.5	0.8834	–	–
9.6 – 10	0.8865	–	–
Extreme rp			
6.4 – 6.7	0.8658	6.4 – 7.9	0.9105
6.8 – 7.2	0.8679	8.0 – 8.3	0.9333
7.3 – 7.5	0.8868	8.4 – 9.5	0.9365
7.6 – 8.4	0.9008	9.6 – 10	0.9396
8.5 – 9.2	0.9038	–	–
9.3 – 9.6	0.9057	–	–
9.7 – 10	0.9075	–	–
Superburst			
6.4	0.8410	6.4 – 6.5	0.9024
6.5 – 7.5	0.8630	6.6 – 10	0.9112
7.6 – 10	0.8669	–	–

The fraction of free neutrons relative to all nucleons  $Y_{\text{nf}}$  can be fitted as a function of pressure  $P$  (at  $P > P_{\text{oi}}$ , for all SGC models) as

$$Y_{\text{nf}} = \frac{y}{1 + ay^3/(1 + 0.88ay^2)}, \quad (\text{A.4})$$

where

$$y = \frac{P}{P_{\text{oi}}} - 1, \quad a = 0.011P_{\text{oi}29}^3. \quad (\text{A.5})$$

The absolute maximum difference of this approximation from the numerical data for all the  $37 \times 3$  considered versions of the SGC models is  $\approx 0.02$ . The approximation (A.4) is shown in Fig. A.1. Here for illustration we show the K model with  $P_{\text{oi}} \approx P_{\text{oi}}^{(0)}$  ( $P_{\text{oi}29} = 7.3$ ), with  $P_{\text{oi}} \approx P_{\text{oi}}^{(\text{cat})}$  ( $P_{\text{oi}29} = 7.9$ ), and with substantially lower and higher values of  $P_{\text{oi}}$  ( $P_{\text{oi}29} = 6.4$  and  $9.5$ ). The inset shows the data (triangles) and the fit (lines) at  $\rho_{\text{oi}} \lesssim \rho \lesssim \rho_{\text{max}}$ , while the main window shows the fit and its extrapolation to the crust bottom. For comparison, Fig. A.1 also shows  $Y_{\text{nf}}$  in three representative models of cold catalyzed crust: BSk22, BSk24, and BSk25 (Pearson et al., 2018). The comparison shows that the extrapolation of the fit is not unreasonable.

## References

Allard, V., Chamel, N., 2024a. Gapless neutron superfluidity can explain the late time cooling of transiently accreting neutron stars. *Phys. Rev. Lett.*, 132, 181001.  
Allard, V., Chamel, N., 2024b. Gapless neutron superfluidity in the crust of the accreting neutron stars KS 1731–260 and MXB 1659–29. *Eur. Phys. J. A*, 60, 116.  
Brown, E.F., 2000. Nuclear heating and melted layers in the inner crust of an accreting neutron star. *Astrophys. J.*, 531, 988.  
Brown, E.F., Cumming, A., 2009. Mapping crustal heating with the cooling light curves of quasi-persistent transients. *Astrophys. J.*, 698, 1020.  
Cackett, E.M., Wijnands, R., Miller, J.M., Brown, E.F., Degenaar, N., 2008. Cooling of the crust in the neutron star low-mass X-ray binary MXB 1659–29. *Astrophys. J.*, 687, L87.

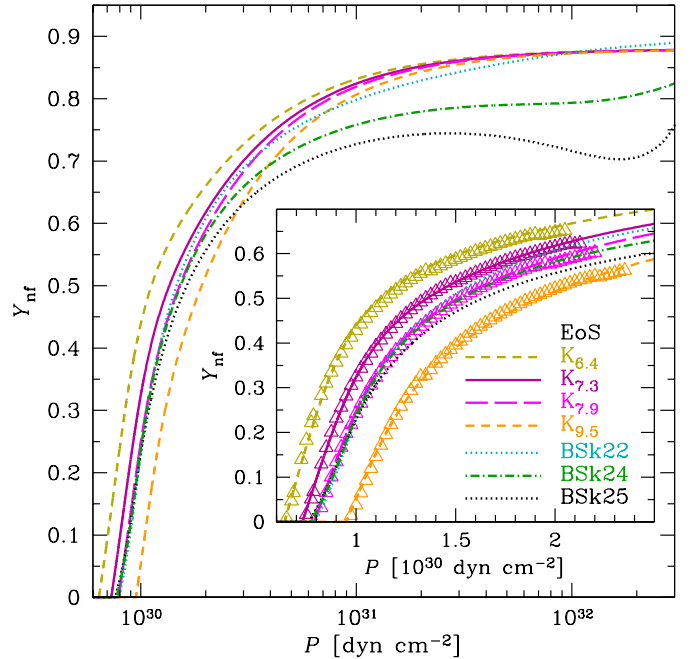


Figure A.1: Dependence of the fraction of free neutrons  $Y_{\text{nf}}$  in the inner crust of a NS on pressure. The inset presents a zoom to the upper part of the inner crust. The lines correspond to analytical approximations, according to the legend: four lines for the SGC accreted crust with  $P_{\text{oi}29} = 6.4, 7.3, 7.9,$  and  $9.5$ , and three ground-state models from the Brussels–Montreal family – BSk22, BSk24, and BSk25. The open triangles in the inset show the numerical SGC results for the K model.

Cackett, E.M., Brown, E.F., Cumming, A., Degenaar, N., Fridriksson, J.K., Homan, J., Miller, J.M., Wijnands, R., 2013. A change in the quiescent X-ray spectrum of the neutron star low-mass X-ray binary MXB 1659–29. *Astrophys. J.*, 774, 131.  
Cyburt, R.H., Amthor, A.M., Heger, A., Johnson, E., Keek, L., Meisel, Z., Schatz, H., Smith, K., 2016. Dependence of X-ray burst models on nuclear reaction rates. *Astrophys. J.*, 830, 55.  
Degenaar, N., Wijnands, R., 2011. The accretion-heated crust of the transiently accreting 11-Hz X-ray pulsar in the globular cluster Terzan 5. *Mon. Not. R. Astron. Soc.*, 414, L50.  
Deibel, A., Cumming, A., Brown, E.F., Reddy, S., 2017. Late-time cooling of neutron star transients and the physics of the inner crust. *Astrophys. J.*, 839, 95.  
Fantina, A.F., Zdunik, J.L., Chamel, N., Pearson, J.M., Haensel, P., Goriely, S., 2018. Crustal heating in accreting neutron stars from the nuclear energy-density functional theory. I. Proton shell effects and neutron-matter constraint. *Astron. Astrophys.*, 620, A105.  
Galloway, D. K., Muno, M. P., Hartman, J. M., Psaltis, D., and Chakrabarty, D., 2008. Thermonuclear (Type I) X-ray bursts observed by the Rossi X-ray Timing Explorer. *Astrophys. J. Suppl. Ser.*, 179, 360.  
Gusakov, M.E., Chugunov, A.I., 2020. Thermodynamically consistent equation of state for an accreted neutron star crust. *Phys. Rev. Lett.*, 124, 191101.  
Gusakov, M.E., Chugunov, A.I., 2021. Heat release in accreting neutron stars. *Phys. Rev. D*, 103, L101301.  
Gusakov, M. E., Chugunov, A. I., 2024. Thermodynamically consistent accreted crust of neutron stars: The role of proton shell effects. *Phys. Rev. D*, 109, 123032.  
Haensel, P., Zdunik, J.L., 1990. Non-equilibrium processes in the crust of an accreting neutron star. *Astron. Astrophys.*, 227, 431.  
Haensel, P., Zdunik, J.L., 2003. Nuclear composition and heating in accreting neutron-star crusts. *Astron. Astrophys.*, 404, L33.  
Haensel, P., Zdunik, J.L., 2008. Models of crustal heating in accreting neutron stars. *Astron. Astrophys.*, 480, 459.  
Heinke, C. O., Zheng, J., Maccarone, T. J., Degenaar, N., Bahramian, A., Sivakoff, G. R. 2024. Catalog of outbursts of neutron star LMXBs.

- arXiv:2407.18867
- Jones, P.B., 1999. Amorphous and heterogeneous phase of neutron star matter. *Phys. Rev. Lett.*, 83, 3589.
- Jones, P.B., 2001. First-principles point-defect calculations for solid neutron star matter. *Mon. Not. R. Astron. Soc.*, 321, 167.
- Keek, L., Heger, A., 2011. Multi-zone models of superbursts from accreting neutron stars. *Astrophys. J.*, 743, 189.
- Mendes, M., Fattoyev, F.J., Cumming, A., Gale, C., 2022. Fast neutrino cooling in the accreting neutron star MXB 1659–29. *Astrophys. J.*, 938, 119.
- Möller, P., Sierk, A., Ichikawa, T., Sagawa, H., 2016. Nuclear ground-state masses and deformations: FRDM(2012). *At. Data Nucl. Data Tables*, 109–110, 1.
- Ootes, L.S., Vats, S., Page, D., Wijnands, R., Parikh, A.S., Degenaar, N., Wijngaarden, M.J.P., Altamirano, D., Bahramian, A., Cackett, E., et al., 2019. Continued cooling of the accretion-heated neutron star crust in the X-ray transient IGR J17480–2446 located in the globular cluster Terzan 5. *Mon. Not. R. Astron. Soc.*, 487, 1447.
- Ortolani, S., Barbuy, B., Bica, E., Zoccali, M., Renzini, A., 2007. Distances of the bulge globular clusters Terzan 5, Liller 1, UKS 1, and Terzan 4 based on HST NICMOS photometry. *Astron. Astrophys.*, 470, 1043.
- Page, D., Reddy, S., 2013. Forecasting neutron star temperatures: predictability and variability. *Phys. Rev. Lett.*, 111, 241102.
- Papitto, A., D’Ai, A., Motta, S., Riggio, A., Burderi, L., Di Salvo, T., Belloni, T., Iaria, R., 2011. The spin and orbit of the newly discovered pulsar IGR J17480–2446. *Astron. Astrophys.*, 526, L3.
- Parikh, A.S., Wijnands, R., Ootes, L.S., Page, D., Degenaar, N., Bahramian, A., Brown, E.F., Cackett, E.M., Cumming, A., Heinke, C., et al., 2019. Consistent accretion-induced heating of the neutron-star crust in MXB 1659–29 during two different outbursts. *Astron. Astrophys.*, 624, A84.
- Pearson, J.M., Chamel, N., Potekhin, A.Y., Fantina, A.F., Ducoin, C., Dutta, A.K., Goriely, S., 2018. Unified equations of state for cold non-accreting neutron stars with Brussels–Montreal functionals – I. Role of symmetry energy. *Mon. Not. R. Astron. Soc.*, 481, 2994; Erratum: 2019, *Mon. Not. R. Astron. Soc.*, 486, 768.
- Potekhin, A.Y., Chabrier, G., 2018. Magnetic neutron star cooling and microphysics. *Astron. Astrophys.*, 609, A74.
- Potekhin, A.Y., Chabrier, G., 2021. Crust structure and thermal evolution of neutron stars in soft X-ray transients. *Astron. Astrophys.*, 645, A102.
- Potekhin, A.Y., Pons, J.A., Page, D., 2015. Neutron stars – cooling and transport. *Space Sci. Rev.*, 191, 239.
- Potekhin, A.Y., Chugunov, A.I., Chabrier, G., 2019. Thermal evolution and quiescent emission of transiently accreting neutron stars. *Astron. Astrophys.*, 629, A88.
- Potekhin, A.Y., Gusakov, M.E., Chugunov, A.I., 2023. Thermal evolution of neutron stars in soft X-ray transients with thermodynamically consistent models of the accreted crust. *Mon. Not. R. Astron. Soc.*, 522, 4830.
- Rutledge, R., Bildsten, L., Brown, E.F., Pavlov, G.G., Zavlin, V.E., Ushomirsky, G., 2002. Crustal emission and the quiescent spectrum of the neutron star in KS 1731–260. *Astrophys. J.*, 580, 413.
- Sato, K., 1979. Nuclear compositions in the inner crust of neutron stars. *Prog. Theor. Phys.*, 62, 957.
- Shchechilin, N.N., Gusakov, M.E., Chugunov, A.I., 2021. Deep crustal heating for realistic compositions of thermonuclear ashes. *Mon. Not. R. Astron. Soc.*, 507, 3860.
- Shchechilin, N.N., Gusakov, M.E., Chugunov, A.I., 2022. Accreting neutron stars: heating of the upper layers of the inner crust. *Mon. Not. R. Astron. Soc.*, 515, L6.
- Shchechilin, N.N., Gusakov, M.E., Chugunov, A.I., 2023. Accreting neutron stars: composition of the upper layers of the inner crust. *Mon. Not. R. Astron. Soc.*, 523, 4643.
- Schatz, H., Aprahamian, A., Barnard, V., Bildsten, L., Cumming, A., Ouellette, M., Rauscher, T., Thielemann, F.-K., Wiescher, M., 2001. The endpoint of the rp-process on accreting neutron stars. *Nucl. Phys. A*, 688, 150.
- Shternin, P.S., Yakovlev, D.G., Haensel, P., Potekhin, A.Y., 2007. Neutron star cooling after deep crustal heating in the X-ray transient KS 1731–260. *Mon. Not. R. Astron. Soc.*, 382, L43.
- Turlione, A., Aguilera, D.N., Pons, J.A., 2015. Quiescent thermal emission from neutron stars in low-mass X-ray binaries. *Astron. Astrophys.*, 577, A5.
- Wijnands, R., Degenaar, N., Page, D., 2013. Testing the deep-crustal heating model using quiescent neutron-star very-faint X-ray transients and the possibility of partially accreted crusts in accreting neutron stars. *Mon. Not. R. Astron. Soc.*, 432, 2366.
- Wijnands, R., Degenaar, N., Page, D., 2017. Cooling of accretion-heated neutron stars. *J. Astron. Astrophys.*, 38, 49.
- Woosley, S.E., Heger, A., Cumming, A., Hoffman, R.D., Pruet, J., Rauscher, T., Fisker, J.L., Schatz, H., Brown, B.A., Wiescher, M., 2004. Models for Type I X-ray bursts with improved nuclear physics. *Astrophys. J. Suppl. Ser.*, 151, 75.